International Journal on Science and Technology (IJSAT)
E-ISSN: 2229-7677 ● Website: www.ijsat.org ● Email: editor@ijsat.org

A Comprehensive Study on the Impact of Fe Ion Concentration on Carbon Steel Corrosion in A CO_2 Environment

Shikha Mishra[1], Sanjay Kumar Singh[2], N.P. Singh[3], Vivke Chauhan[4]

[1]Research scholar, Department of Chemistry, Mansarovar Global University, Bhopal (M.P.)
[2,3]Associate Professor, Department of Chemistry, DBS P.G. College Govind Nagar Kanpur (U.P.)
[4]Assistant Professor, Department of Paramedical Sciences, Vivekananda Global University, Jaipur (Rajasthan)

Abstract
In this work, the corrosion behaviour of steel wires in solutions containing different concentrations of Fe^{2+} was investigated, while the evolution of pH was monitored in-situ and changes of the Fe^{2+} concentration were monitored ex-situ. Characterization of the corrosion scales was performed by using microscopic and diffraction techniques. Scale analysis revealed that the passivation of samples, exposed to initially highly Fe^{2+} super-saturated solution, occurred when a formation of a double layer took place, resulting in 30 times lower corrosion rate compared to samples tested in solutions without initial Fe^{2+}.

Keywords: Carbon Steel, Carbon Dioxide

1. Introduction

Corrosion of materials has continued to receive interest in the technological world. In the field of corrosion inhibition, scientists are persistent in seeking better and more efficient ways of combating the corrosion of metals. Addition of corrosion inhibitors to the corrosion environment with respect to the other methods of corrosion inhibition has been employed (Orubite et al., 2007). Corrosion inhibition of materials has been the focus of research for centuries and in many cases has been well analysed and understood (Maksoud, 2008). The use of inhibitors is one of the most practical methods for protection against corrosion in acidic media. Corrosion of materials usually takes place in the presence of oxygen and moisture and involves two electrochemical reactions, oxidation occurs at anodic site and reduction occurs at cathodic site (Kumar, 2008). Various scientific studies deal with the subject of corrosion inhibitors. Inhibitors are normally used to protect materials against deterioration from corrosion. These organic compounds have multiple bonds in their molecules that mainly contain nitrogen, sulphur, oxygen atoms through which they get adsorbed on the metal surface (Kumar, 2008). The use of ethoxylated fatty acid, ethoxylated fatty amines, and propenethoxylated diol had been used as corrosion inhibitors for steel and aluminium in acidic solutions. Effect of temperature on the inhibiting process is of enormous significance in industry (Zarrouk et al., 2010). Effective inhibitors are expected to perform under a wide range of conditions. The inhibition efficiency depends on the parameters of the system (temperature, pH, duration, and metal composition) and on the structure of the inhibitor molecule. Flexible pipes consist of concentric layers of polymers and steel, which are not bonded together to

preserve the flexibility of the pipe (Rubin and Gudme, 2006). The fatigue resistance of tensile armours is determined by the applied stresses and operating corrosive environment (Rubin and Gudme, 2006). As a result of diffusion of small molecules such as methane (CH_4), carbon dioxide (CO_2), hydrogen sulphide (H_2S), and water (H_2O) through the inner liner into the annulus, corrosion of steel armours might occur. The confined environment, which steel armours are exposed to in the annulus region, is characterized by a low ratio of free water volume (V) to steel surface area (S), typically below 0.1 ml cm^{-2}. Under corrosive conditions, the low V/S ratio results in a fast supersaturating of Fe^{2+} in the liquid and corrosion rates are typically below 10µm/year. In the annulus region, unlike bore conditions, there is no vigorous flow of water and even though the pipe moves due to waves and water current, it is believed that conditions are relatively stagnant. In the aqueous CO_2 environment, the corrosion process of carbon steel occurs through an electrochemical process, which involves dissolution of iron and cathodic evolution of hydrogen (Nesic, 2007). In the presence of CO_2, the corrosion rate of carbon steel is increased by a corresponding increase of the rate of the hydrogen evolution reaction (Nesic, 2007). It has been reported (Nesic, 2007) that cathodic reactions, which take place in aqueous CO_2 environment, contain two independent reactions, such as hydrogen reduction and carbonic acid reduction (H_2CO_3). It is, however, still not certain whether the H_2CO_3 is directly reduced or whether it dissociates to form bicarbonate (HCO_3^-).

2. Materials and methodology

2.1. Experimental setup for corrosion testing: - The experimental setup consisted of a de-aeration vessel, a pre-corrosion vessel, and an electrochemical cell. All vessels were made of glass and equipped with 316L steel tubing to avoid any ingress of oxygen. The electrochemical cell contained a saturated calomel electrode (REF 421 Reference Electrode, Calomel) as a reference electrode, a platinum counter electrode with a surface area of 310 cm^2, and a rectangular carbon steel specimen as a working electrode with a surface area of 6 cm^2. Apart from the working electrode, the electrochemical cell had three additional samples (each 49.5 cm^2), which were used for the scale analysis and one weight loss coupon used for mass loss determination (6 cm^2). Additionally, the setup was equipped with a pH electrode to monitor the pH changes during the entire test.

2.2. Material and specimen preparation:-The material used for the electrochemical experiments was carbon steel with a composition of 0.77 wt-% C, 0.24 wt-% Si, 0.65 wt-% Mn, 0.17 wt-% P, 0.06 wt-% S, Fe as the balance. The yield strength of the material is 1350 MPa. As-received, from cold rolling process (Ra = 0.38 ± 0.05 µm), surface conditions are used for the experiment to simulate material conditions under use in flexible pipes. Prior to each experiment, the electrode surface was thoroughly degreased with acetone, cleaned with ethanol, and dried in a hot air flow.

2.3. Electrolyte solution:-Electrochemical experiments were conducted in artificial seawater with a chemical composition according to ASTM D1141 (Table 2), under 1 bar CO_2 conditions. The flow rate of CO_2 gas was 250 ml min^{-1}. The temperature of the electrolyte solution was set to 20±1°C. The solution was de-aerated in the de-aeration vessel by purging nitrogen gas until the oxygen content was lower than 5 ppb. The dissolved oxygen was measured by using optical oxygen sensor. The whole setup was flushed with nitrogen in order to remove any oxygen. Electrochemical experiments were carried out with four starting Fe^{2+} concentrations namely: 0 mg L^{-1}, 370 mg L-^{1}, 514 mg L^{-1}, and 1300 mg L^{-1} (the last concentration refers to the high super-saturation condition). The corresponding alkalinity (HCO_3^- concentration) of the test solutions is shown in Table 3. In order to generate electrolytes containing

different concentrations of Fe^{2+}, steel wool was exposed to de-aerated seawater under 1 bar CO_2 in the pre-corrosion vessel for different periods of time. Due to corrosion of the steel wool, the generation of Fe^{2+} together with HCO_3^- took place. When the solution obtained a specific Fe^{2+} concentration, it was transported to the test vessel. The Fe^{2+} contents were measured by ultraviolet-visible spectrophotometry method using a Shimadzu UV-1800 Spectrophotometer, with an error margin of 1 %. The pH of the test solutions was measured using a pH meter. The water free volume to steel area ratio was 24 ml cm^{-2} during all the experiments. The volume of the test solution was 3.8 L. In order to ensure the homogenous bulk solution mixing, the electrolyte was stirred at 350 rev min^{-1}. Details of test solutions are listed in Table 3.

2.4. Electrochemical measurements:-In order to perform electrochemical measurements, the CH Instruments Electrochemical Analyser potentiostat together with CHI602b software were used. Linear Polarization Resistance (LPR) measurements were carried out as a function of exposure time on the same sample during continued exposure. Potentials were scanned between - 20 to 20 mV vs. open-circuit potential at a scan rate of 0.166 mv s^{-1}. All potentials were measured with respect to SCE. The intersection of the anodic and cathodic part was measured as E_{corr}. The area-averaged corrosion current density is calculated according, where B is the Stearn-Geary constant, Rp is the polarization resistance and A is the area of the specimen.25 For each tested sample, the B value was calibrated, so that the integral material loss, found from the LPR measurements, fitted with the weight loss obtained experimentally (Table 1). Depending on the exposure conditions, the B values varied from 20 to 27 mV.

2.5. Scale analysis:-To assess the morphology of the resulting corrosion scales, cross sections of the exposed samples were metallographically prepared and investigated by means of scanning electron microscopy using secondary electrons (SE) and back-scattered electrons (BE). Qualitative phase analysis of the corrosion products was performed by means of X-ray Diffraction (XRD, Bruker AXS Diffractometer D8 Discover). Measurements were performed with Cr-Kα radiation and carried out on the surface of the samples resulting in a penetration depth of up to 17 µm.

2.6. Thermodynamic calculations:-Thermodynamic calculations were performed with the commercially available Multiscale model (version 8.1) to calculate the solubility limit of $FeCO_3$ and saturation ratio (SR) with respect to $FeCO_3$, for different Fe^{2+} and corresponding HCO_3^- concentrations (Table 4). Calculations were performed for artificial seawater with a chemical composition according to the ASTM D1141 standard (Table 2) at 1 bar CO_2 at 20°C.

Initial Fe2+ in the experiments (mg L^{-1})	**Test exposure (h)**	**Corrosion rate (µm/year)**
0	242	1339
370	242	788
1300	242	373
514	4485	165
1300	1613	33

Table 1:- The results of corrosion rates from weight loss measurements

	NaCl	$MgCl_2$	Na_2SO_4	$CaCl_2$	KCl	$NaHCO_3$	KBr	H_3BO_3	$SrCl_2$	NaF
Composition ($mg\ L^{-1}$)	24530	5200	4090	1160	695	201	101	27	25	3

Table 2:- Chemical composition of Seawater (ASTM D1141).

Base solution	Fe^{2+} ($mg\ L^{-1}$)	HCO_3^- ($mg\ L^{-1}$)	pH	Temperature (°C)	Oxygen (ppb)	Exposure time (h)
Artificial	0	61*	4.7	20	< 5	242
	370	869	5.6			242
Seawater	514	1184	5.7			4485
	1300	2901	6.2			242, 1613

Table 3 Details of test solutions and conditions. * HCO_3^- concentration in pure Seawater

Fe^{2+} ($mg\ L^{-1}$)	0	100	200	370	500	700	900	1100	1300
HCO_3^- ($mg\ L^{-1}$)	61	279.5	497.9	869.3	1153.3	1590.2	2027.1	2464.1	2901

Table 4 Concentrations of Fe^{2+} and HCO_3^- used for Multiscale calculations.

3. Results

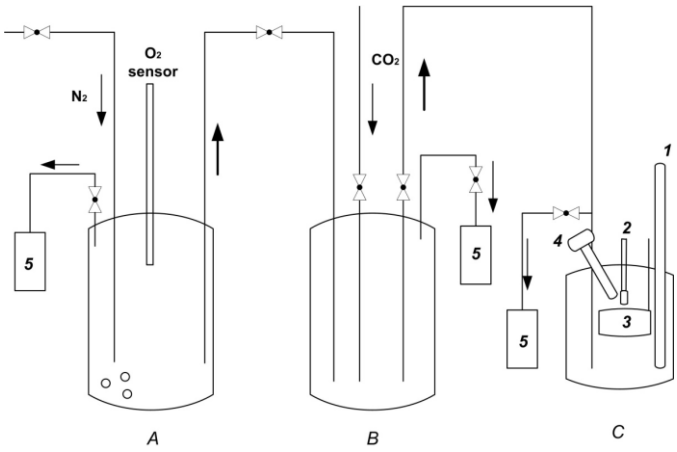

Figure 1:- Schematic drawing of the test set-up for corrosion testing: (A) De-aeration chamber, (B) Pre-corrosion chamber, (C) Electrochemical cell ((1) pH electrode, (2) Working electrode, (3) Counter electrode, (4) Reference electrode, and (5) Wash bottle).

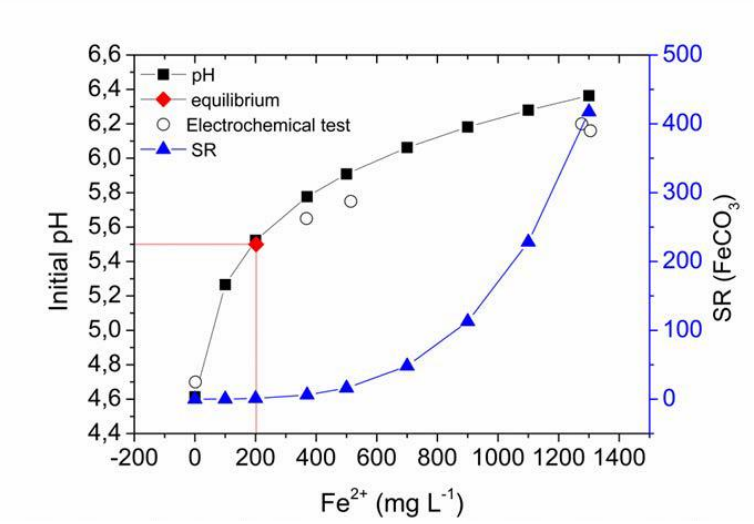

Figure 2:- Thermodynamic calculations made in Multiscale model together with initial pH and Fe^{2+} concentrations from electrochemical experiments

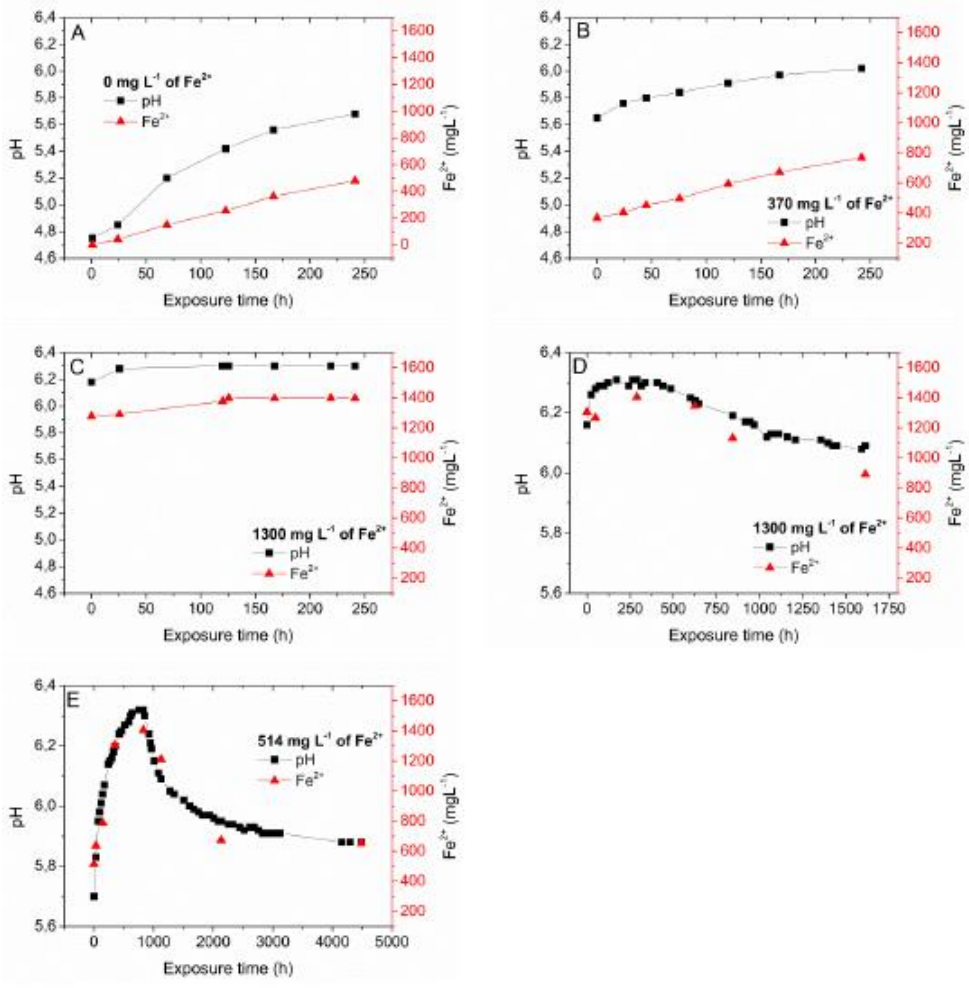

Figure 3:- Evolution of the Fe^{2+} content (right axis) and pH (left axis) for tests performed in solutions with initial Fe^{2+} content of A) 0 mg L^{-1}, B) 370 mg L^{-1}, C) 1300 mg L^{-1} for 242 hours D) 1300 mg L^{-1} for 1613 hours of exposure, and E) 514 mg L^{-1} for 4485 hours of exposure.

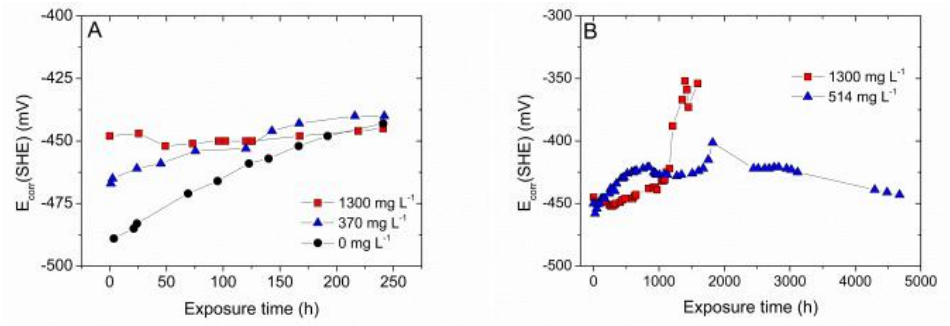

Figure 4:- Evolution of E_{corr} as a function of time for exposure tests with different initial Fe^{2+} content that were running for A) 242 hours and B) 1613 hours and 4485 hours.

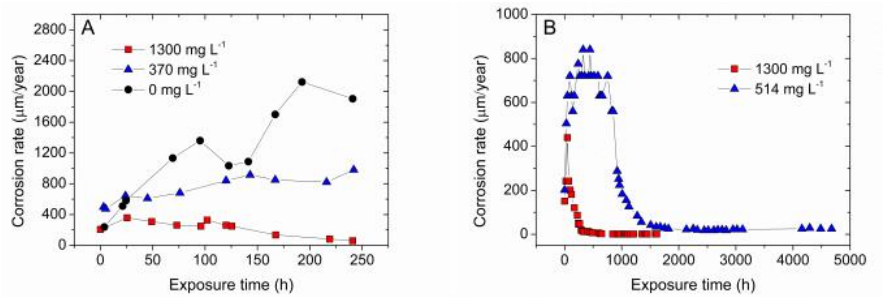

Figure 5:- Corrosion rates as a function of time for tests with different initial Fe^{2+} content that were running for A) 242 hours and B) 1613 hours and 4485 hours.

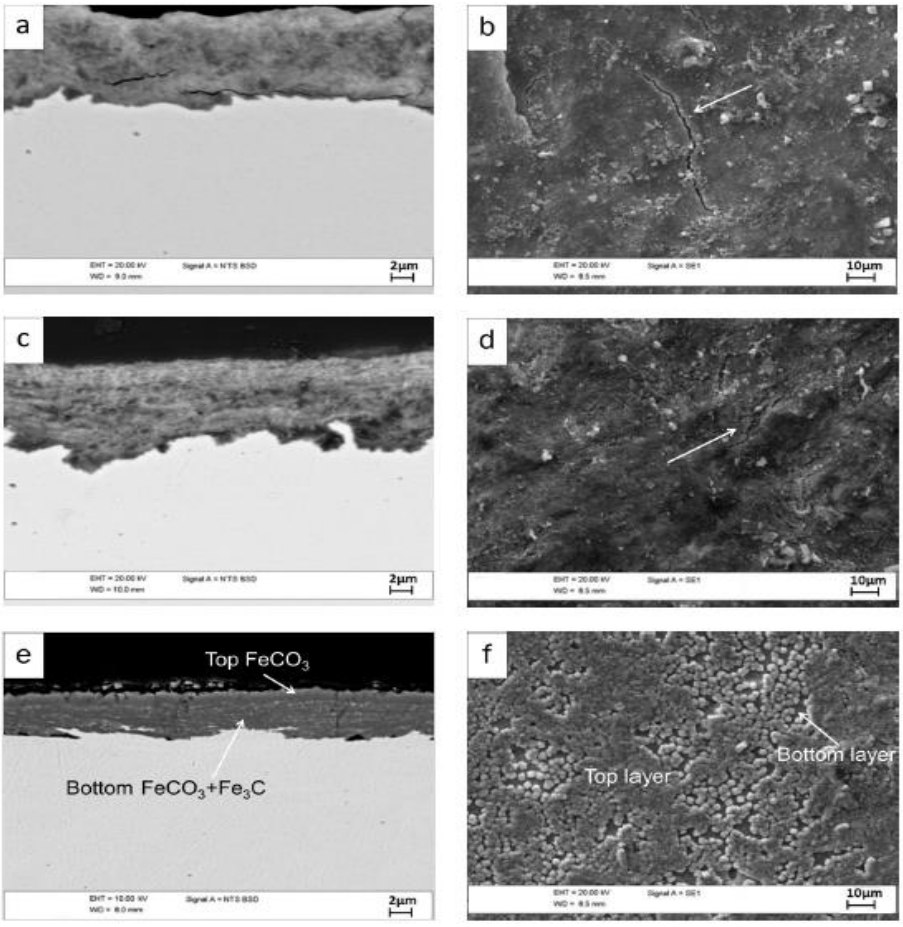

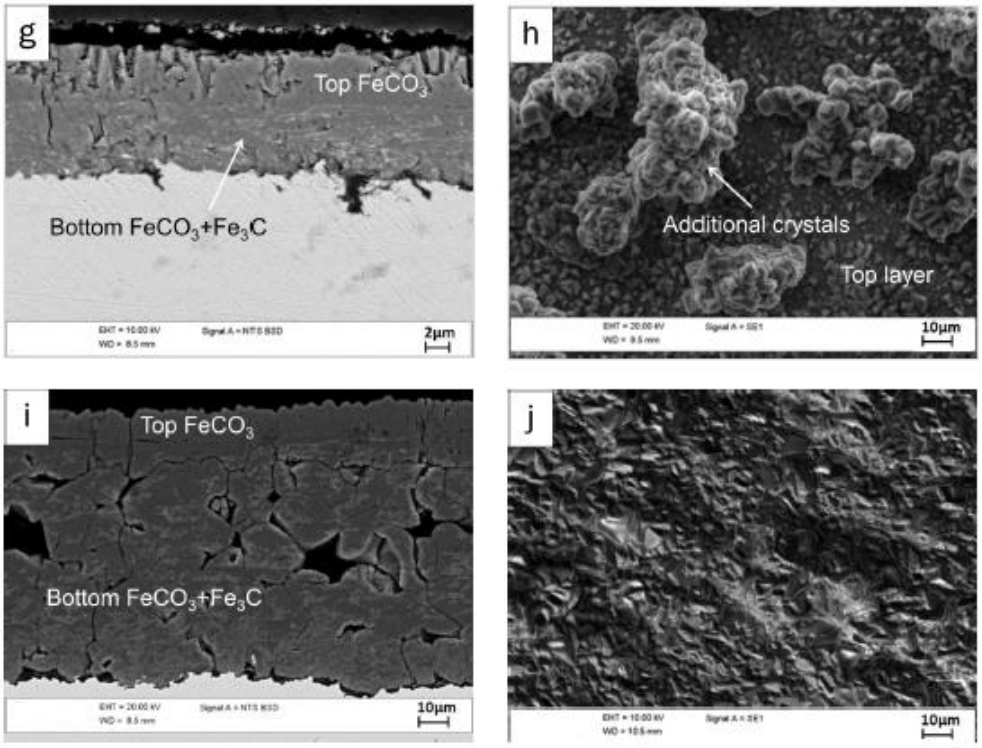

Figure 6:- Cross sectional and top surface morphologies of corrosion scales formed in solutions with initial Fe^{2+} content of 0 mg L^{-1} (a and b), 370 mg L^{-1} (c and d), 1300 mg L^{-1} for 242 hours (e and f) and 1300 mg L^{-1} for 1613 hours (g and h) and 514 mg L^{-1} for 4485 hours.

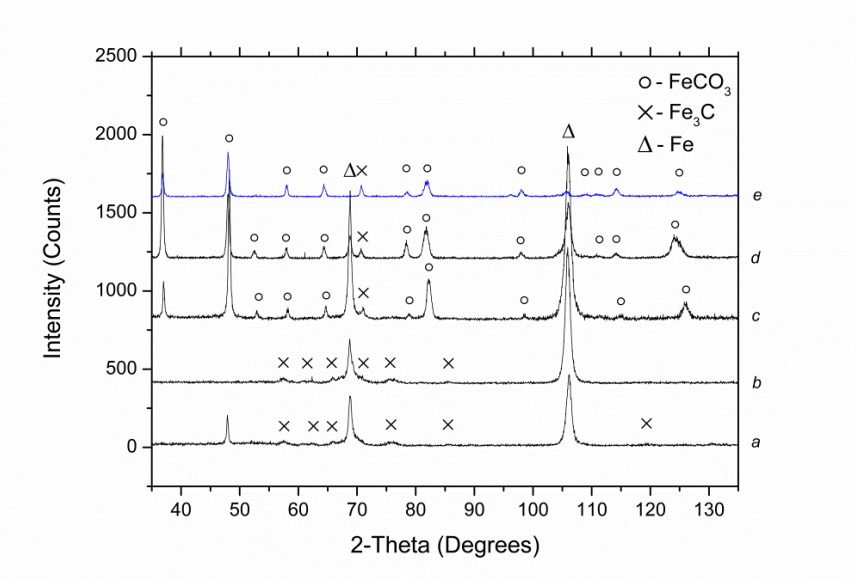

Figure 7:- XRD analysis of corrosion scales formed in solutions with initial Fe^{2+} content of 0 mg L^{-1} (a), 370 mg L^{-1} (b), 1300 mg L^{-1} for 242 hours (c) and 1300 mg L^{-1} for 1613 hours (d) and 514 mg L^{-1} for 4485 hours (e).

Thermodynamic calculations:- Fig. 2 presents thermodynamic calculations of pH and saturation ratio (SR) with respect to $FeCO_3$ as a function of the initial Fe^{2+} and HCO_3^- concentration together with the experimental data obtained from the solution analysis of the electrolyte used for electrochemical testing. The solubility limit of $FeCO_3$, calculated by the Multiscale model, in 1 bar CO_2 at 20°C was equal to 202

mg L^{-1} of Fe^{2+} and the pH 5.5. Results revealed that for all experiments of the present work, super saturated conditions existed except for the experiment with initial pH of 4.7 and 0 mg L^{-1} of Fe^{2+}. Calculated results also showed that by increasing the initial Fe^{2+} and HCO_3^- content in the electrolyte, the SR was similarly increased. It was shown that pH was increasing with Fe^{2+} concentration, which was directly related to increasing HCO_3^- content in the solution. Overall, the pH measured from the electrochemical experiments and the corresponding Fe^{2+} content were in a good agreement with the calculations.

3.1 Electrochemical testing and electrolyte analysis:-Evolution of Fe^{2+} and pH:-Fig. 3 presents the evolution of pH and Fe^{2+} as a function of exposure time in the solutions with various initial Fe^{2+} concentrations. The trends of pH evolutions were observed to follow changes in Fe^{2+} concentrations as a direct consequence of changing the HCO_3^- concentration in the solution. Results from the tests without initial Fe^{2+} (Fig. 3 A) and with 370 mg L^{-1} of Fe^{2+} (Fig. 3 B) showed that the pH increased simultaneously with an increase in the Fe^{2+} content in the solution during the time of exposure. Results shown in Fig. 3 C (highly super saturated condition) showed that the pH increased at the beginning of the test and stabilized after 125 hours. However, it should be noticed that no data is available between 25 and 125 hours, so stabilization could have occurred earlier. For the prolonged test with initially high super saturated conditions (Fig. 3 D) and 514 mg L^{-1} of Fe^{2+} (Fig. 3 E), pH increased until it reached a maximum level of 6.3 after 250 hours and 921 hours, respectively, and it decreased with further exposure time and so the Fe^{2+} concentration does as well.

3.2 Evolution of the corrosion potential:-To further explore the impact of Fe^{2+} concentrations and pH changes on the electrochemical behaviour of the material and its scale formation, the evolution of the corrosion potential (E_{corr}) was analysed. The curves in Fig. 4 clearly show that the initial E_{corr} values were influenced by different initial Fe^{2+} concentration in the corrosive media. The E_{corr} value for the experiment with highest concentration of Fe^{2+} in the solution had more positive potential in the beginning of the test compared to potentials measured in solutions without initial Fe^{2+} and with 370 mg L^{-1} (Fig. 4 A). For experiments without initial Fe^{2+} and with 370 mg L^{-1} of Fe^{2+}, E_{corr} increased as a function of exposure time and stabilized after approximately 167 and 75 hours, respectively. For the sample exposed to the highly supersaturated solution (1300 mg L^{-1}), the measured potential revealed a constant value of -450 mV during the whole test and after approximately 440 hours it started to drift towards more positive values (Fig. 4 B). Further, the corrosion potential for the sample exposed to the solution with 514 mg L^{-1} of Fe^{2+} (Fig. 4 B) increased at the beginning of the test, and after 1820 hours it began declining again reaching the final value of approximately -440 mV. The corrosion potentials measured in the experiments are higher compared to the theoretical values obtained from the Nernst equation, where the potential varies from -670 mV up to -580 mV for Fe^{2+} content of 1 mg L^{-1} and 1300 mg L^{-1}, respectively. The calculated potentials represent theoretical equilibrium conditions and in this case, only take the impact of the Fe^{2+} concentration on the obtained potential into account. However, in the experiments presented in this paper, the equilibrium was not obtained. Additionally, the potential obtained experimentally in the present tests, was not only influenced by the concentration of Fe^{2+} but also by the formation of corrosion scale and its protective properties, which could explain differences between experimentally measured and theoretical potentials.

3.3 Corrosion rates: - Fig. 5 presents the corrosion rates as a function of exposure time for samples exposed to solutions with various initial Fe^{2+} concentrations. The maximum corrosion rate was observed for samples tested in solutions containing no initial Fe^{2+} (0 mg L-1), where the corrosion rate increased

as a function of time and reached 1905 µm/year (Fig. 5 A). The addition of 370 mg L^{-1} of Fe^{2+} to the solution decreased the final corrosion rate to 981 µm/year (Fig. 5 A). A decrease of the corrosion rate in CO_2 environment with time was first observed when exposing samples to highly supersaturated solution: corrosion rates of 60 µm/year were obtained after 242 hours (Fig. 5 A) and 1.5 µm/year after approximately 440 hours of exposure (Fig. 5 B), which correlates very well with increasing corrosion potential after approximately the same time of exposure, as shown in Fig. 4 B. Electrochemical experiments revealed that the time needed to obtain a decrease in corrosion rate is considerably longer for the sample exposed to the solution with 514 mg L^{-1} (826 hours) than the one with 1300 mg L^{-1} (48 hours) (Fig. 5 B). It should be noticed that for samples tested in a solution with an initial Fe^{2+} content of 514 mg L^{-1}, a decrease in corrosion rate occurred approximately at the same time when the maximum Fe^{2+} concentration and pH was reached, as presented in Fig. 3 E.

3.4 SEM and XRD analysis:-The top surface and cross-sectional morphologies of the corrosion scales formed in solutions with various initial Fe^{2+} concentrations are shown in Fig. 6. The thickness of the layer decreased with increase in initial Fe^{2+} content (~ 12 µm for solutions with no initial Fe^{2+} (Fig. 6 a) and ~5 µm in highly super saturated environment (Fig. 6 e). Depending on the exposure conditions, the corrosion scales exhibited differences in morphologies. For samples exposed to solutions without initial Fe^{2+} and with 370 mg L^{-1} of Fe2+ , the corrosion scales had similar characteristics and were composed of light grey phases integrated in a darker matrix (Fig. 6 a and c). This indicated that there was a chemical difference between these two regions and the corrosion layer must have contained two different phases. The XRD measurements (see Fig. 7) revealed many cementite (Fe_3C) peaks for samples exposed to solutions without Fe^{2+} and with 370 mg L^{-1} of Fe^{2+}. A single $FeCO_3$ peak was also detected when testing with 0 mg L^{-1} of Fe^{2+}, which is in contrast to the sample exposed to the solution with 370 mg L^{-1} Fe^{2+}, where no $FeCO_3$ could be detected. Additionally, the top surface scale analysis did not show characteristic $FeCO_3$ crystals for samples exposed to 0 mg L^{-1} and 370 mg L^{-1} Fe^{2+} (see Fig. 6 b and d, respectively). This might indicate that either the crystals were too small to see with the resolution used in this paper due to short exposure time, or there was another corrosion product formed with a non-crystalline structure, which would not be detectible with XRD. Consequently, it can be concluded that the corrosion scale formed in a solution with an initial Fe^{2+} of 0 mg L^{-1} and 370 mg L^{-1} consisted of Fe_3C originating from the steel embedded in a corrosion product, which could be $FeCO_3$ (for 0 mg L^{-1} of Fe^{2+}) or non-crystalline phase. Due to the higher X-ray penetration depth (17 µm for high diffraction angles) compared to the thicknesses of these scales, it cannot be excluded that some Fe_3C was measured from the substrate of the material. Surface analysis also revealed some cracks formed in the corrosion scales, which are seen in Fig. 6 b and d, which are mostly likely formed during preparation of the samples. When exposing the samples to highly supersaturated solutions, a dense double-layered scale was formed (Fig. 6 e). It consisted of an upper, homogeneous layer and a bottom, inhomogeneous layer, which was also observed for samples tested in solutions with no initial Fe^{2+} and with 370 mg L^{-1} of Fe^{2+} (Fig. 6 a and c, respectively), with light grey regions integrated in the darker matrix. The SEM analysis revealed protrusions of corrosion products with more compact scale beneath (Fig. 6 f). The sample exposed to highly super saturated solution for a prolonged time (Fig. 6 g) also showed the formation of a double layer with additional protrusions on the top (Fig. 6 h). Due to extended exposure time, the corrosion scale was approximately twice the thickness compared to the scale formed after exposing for 242 hours. Formation of a double-layered scale was also observed for the sample exposed to the solution initially containing 514 m L^{-1} of Fe^{2+} (Fig. 6 i). The bottom layer was seven

times thicker in the solution with 514 mg L^{-1} (Fig. 6 i) than in 1300 mg L^{-1} of Fe^{2+} (Fig. 6 g). Many cracks and pores were also present in the bottom part of the scale, while a compact and thin layer covering the bottom layer was formed on the top (Fig. 6 i and j). XRD results showed that a number of $FeCO_3$ peaks with high intensities were detected for samples exposed to highly super saturated solutions (Fig. 7 patterns c and d) and electrolytes with 514 mg L^{-1} of Fe^{2+} (Fig. 7 e). This indicated that the volume fraction of this phase was much larger than obtained for the two other scales formed in solutions without iron ions and 370 mg L^{-1} of Fe^{2+} (Fig. 7 a and b, respectively). Further, there was a shift in the position of a $FeCO_3$ peaks for samples exposed to highly super saturated solution (Fig. 7 d) and with 514 mg L^{-1} of Fe^{2+} (Fig. 7 e) compared to peaks recorded for samples exposed to solutions without Fe^{2+} (Fig. 7 a) and with 370 mg L^{-1} Fe^{2+} (Fig. 7 b): peaks were shifted towards lower diffraction angles indicating changes of the state of internal stresses, compared to those detected in pattern a and c in Fig. 7. The XRD measurements also revealed the presence of Fe_3C. However, only a single Fe_3C peak with low intensity was detected for samples tested in highly super saturated solutions (Fig. 7 c and d) and 514 mg L^{-1} (Fig. 7 e). Due to the large thickness of the corrosion scale formed in a solution with 514 mg L^{-1} of Fe^{2+}, compared to the maximum penetration depth of the X-ray beam (17 μm), it can be concluded that the Fe_3C phase was present in the corrosion scale. This, together with the observed morphology of the corrosion scale, indicated that the bottom layer consisted of Fe_3C integrated in a $FeCO_3$ matrix, while the top layer contained only $FeCO_3$ phase, as shown in Fig. 6 i. This is also applicable for double scales formed in highly super saturated solutions (Fig. 6 e and g) and confirms the results discussed above, i.e. that the Fe_3C measured from solutions with no Fe^{2+} and 370 mg L^{-1}, indeed, originated from the corrosion scale and not the substrate.

4 Discussion:

Overall analysis of the results showed that the initial concentration of Fe^{2+} and HCO_3^-, together with resulting pH, in the solution had a significant impact on the electrochemical behaviour of steel, corrosion rate, and scale formation. It is important to emphasize that it is not the concentration of Fe^{2+} that directly affects the corrosion rate, but the kinetics of scale formation and its morphology are influenced by the initial concentration of Fe^{2+}, as shown by the results.It was shown that the general corrosion rate decreased when increasing the initial concentration of Fe^{2+} in the solution, which is in agreement with formerly published results.3,13,14,17 Despite of the formation of a relatively thick corrosion scale (12 μm), which was formed in solutions with no initial Fe^{2+} and 370 mg L^{-1}, the scale was not protective, which was reflected in the increasing corrosion rates with the exposure time, even though the saturation level for $FeCO_3$ was exceeded in both tests. Current results, from the tests performed with initial Fe^{2+} concentration of 0 and 370 mg L^{-1}, confirm that protectiveness of the formed corrosion scale depends more on its structure and morphology rather than on thickness and the scales formed at room temperature can be even 100 μm thick and still non-protective (Nordsveen et al., 2003). At room temperature, the process of $FeCO_3$ precipitation is much slower compared to high temperatures (above 60^{o}C) and when the corrosion rate is faster than the scale formation, a porous and non-protective corrosion layer is developed (Nordsveen et al., 2003). However, based on the SEM analysis, no porosity was seen for scales formed in solutions with an initial Fe^{2+} of 0 mf L^{-1} and 370 mg L^{-1}. Han et al., (2007) have reported that due to non-uniform formation of a corrosion scale, a galvanic effect between film-covered surface (cathode) and uncovered parts of metal surface (anode) enhanced the corrosion rate of steel; this might have also taken place for samples tested in solutions with an initial Fe^{2+} of 0 mg L^{-1} and

370 mg L^{-1}, which would explain their increasing corrosion rate with exposure time. SEM analysis showed that for samples exposed to solutions with an initial Fe^{2+} of 0 mg L^{-1} and 370 mg L-1, a single corrosion layer was formed, which consisted of Fe_3C embedded in a corrosion product. XRD analysis, performed for samples exposed to solutions with 0 mg L^{-1} Fe^{2+} suggested that the scale consisted of Fe_3C embedded in $FeCO_3$ matrix, which was also reported by Berntsen et al., (2013). However, corrosion scale did not have typical $FeCO_3$ crystals, which might indicate either that the crystals, were too small to be seen with the used resolution, or that another corrosion product was formed as well. It has been reported (Han et al., 2008) that one of the corrosion products formed in aqueous CO_2 environment was ferrous hydroxide ($Fe(OH)_2$), which might not have a crystalline structure and thus could not be detected with XRD. Since both scales have a similar morphology, it is expected that both scales consisted of Fe_3C originating from the steel embedded in a corrosion product of $Fe(OH)_2$ and/or $FeCO_3$. Cementite (Fe_3C) is a second predominant phase in the corrosion scale formed in aqueous CO_2 environment. In a ferritic-pearlitic microstructure, cementite is considered as non-corroding part of steel and may become a site for cathodic reactions (Han et al., 2008), which lead to micro galvanic coupling between the Fe_3C and ferrite (α-Fe) and consequently increasing corrosion rates. This was confirmed by Mora and Turgoose (2002), where it has been shown that the corrosion rate of mild steel in CO_2 solution with pH 5.5 increased with exposure time as a results of un-oxidized Fe_3C and its galvanic effect on the corrosion rate. Berntsen et al., (2013) have reported that due to preferential dissolution of ferrite (α-Fe), Fe_3C accumulates on the surface and becomes embedded in the $FeCO_3$ film. Crolet et al., (1998) that the main difference between protective and non-protective morphologies of the corrosion scales formed in aqueous CO_2 environment is the presence of empty cementite (Fe_3C) layer in contact with steel surface in case of non-protective scales and fill of Fe_3C network with $FeCO_3$ in case of protective corrosion layers. However, despite of a clear increase in corrosion rate, which indicated formation of non-protective scales for samples tested in solutions with initial Fe^{2+} concentration of 0 mg L^{-1} and 370 mg L^{-1}, no empty Fe_3C layer was observed close to the metal surface with the SEM resolution employed in this paper. With the generation of the test solution with a high supersaturation of Fe^{2+} by corrosion of steel wool under CO_2 sparging, a large concentration of Fe^{2+} and the equivalent amount of HCO_3^- was created. After transfer of the test solution to the test vessel, only the corrosion of the test specimens could provide additional Fe^{2+} to the solution. It was shown that such conditions lead to a formation of a protective corrosion scale and very low corrosion rates of 1.5 μm/year, in accordance with the practical experience with flexible pipe. Decrease in corrosion rate was also seen in a solution containing initially 514 mg L^{-1} of Fe^{2+}, but the minimum corrosion rate of 25 μm/year was first seen after 2324 hours. Results from tests performed with solutions highly supersaturated with Fe^{2+}, showed that a double layer scale was formed. It was clear that high initial Fe^{2+} concentration facilitated formation of a dense and protective scale, which was reflected in a decreased corrosion rate and increased corrosion potentials. These results are in a good agreement with already published data (Han et al., 2008) where it was shown that by exposing samples to solution initially highly supersaturated with Fe^{2+}, thus by providing high SR, a rapid reduction of the corrosion rate was seen due to the formation of protective corrosion layer. It is known that higher supersaturation of Fe^{2+} increases the rate of a formation of $FeCO_3$ scale (Dugstad, 2006) which might have also taken place when exposing samples to solutions with Fe^{2+} of 1300 mg L^{-1}, which would support the statement that high supersaturation of Fe^{2+} is necessary for the formation of protective films (Videm and Dugstad, 1989). The thermodynamic calculations presented in the present paper support this observation where the saturation ratio of $FeCO_3$, which is a driving force of scale

formation,20 was much higher in solutions with 1300 mg L^{-1} (SR=417) than in solutions with 370 mg L^{-1} (SR=6) and 514 mg L^{-1} of Fe^{2+} (SR=16). Based on the detected phases by XRD measurements, it is likely that a bottom layer of corrosion product consisted of Fe_3C integrated in a $FeCO_3$ matrix and the top layer contains only the $FeCO_3$ phase. It has been reported (Ueda and Ikeda, 1996) that the formation of $FeCO_3$ is associated with the steel microstructure. The steel used for this investigation has a microstructure with a very fine dispersion of Fe_3C in ferrite with less than 10% by volume of carbide-free ferrite. Ferrite grains are relatively small (2-5 μm) and widely distributed. According to Al-Hassan et.al., (1998) due to more positive potential of Fe_3C, cementite does not corrode and provides effective cathodes, thus in the present steel cathodes are abundant even on the most local scales. Since the cementite (Fe_3C) does not dissolve, it will provide a good geometrical marker for the location of the original surface. With the observed two-layer scale, the outer (top) layer consisting only of $FeCO_3$ with no cementite may have grown at least partly by precipitation from the solution, which could explain decreasing concentration of Fe^{2+} in the electrolyte with time, as it was also reported by Berntsen et al., (2013). It cannot, however, be excluded that Fe^{2+} may also be provided by diffusion from the steel side. The present study does not allow a distinction between the two possible sources of Fe^{2+}. It is believed that the $FeCO_3$ present in the bottom layer was primarily formed from the Fe^{2+} due to dissolution of the steel substrate, which explains the presence of Fe_3C originating from the steel in the scale, but certainly Fe^{2+} present in the bulk solution also contributed to the process of scale formation. It is suggested that the interface between the bottom and the top layer presents the original surface of the material. The formation a double layer has been also reported by Dugstad et al., (2015) when exposing steel armours used in flexible pipes to artificial seawater, with a high initial Fe^{2+} concentration of 2000 ppm, at 1 bar CO_2. The corrosion layer consisted of an inner layer, which consisted of $FeCO_3$ and Fe_3C together with alloying elements originating from the steel, and an outer layer of $FeCO_3$ precipitated from the Fe^{2+} in the solution. A similar morphology of the corrosion scale was also reported by Gao et al., (2011) where experimental and SEM results showed that by performing tests at 10 bar CO_2 at 75ºC and pH 6.5, a formation of double layer corrosion film took place. Similar to current results, the two layers were divided by a straight line, which represented the initial surface of the material. Gao et al., (2011) has reported that the layer formed closer to the metal surface had a two-phase structure and a higher resistance compared to the outer homogenous layer. Results from extended exposure to highly supersaturated solutions with Fe^{2+} showed that the scale became even more protective with time. It is in a good agreement with formerly published results (Zhang et al., 2012), where it has been shown that the surface coverage percentage by $FeCO_3$ increased with exposure time, and at the same time the corrosion scale became denser and more protective. Formation of a double layer, with a similar morphology compared to the scale formed in highly supersaturated conditions, was also seen for the sample exposed to the solution with 514 mg L^{-1} of Fe^{2+}. However, the thickness of the bottom part of the scale was seven times larger than the one formed in highly super saturated solution, which was also reflected in the extended time needed for the corrosion rate to decrease. The XRD measurements revealed a shift in the position of $FeCO_3$ peaks, similar to the pattern obtained for samples exposed to solutions initially highly super saturated with Fe^{2+} for a prolonged time. The shift in the $FeCO_3$ peaks position is most likely related to the presence of compressive stresses in the formed scale. It might be that the level of stress, which was high enough to be visible in a peak shift in XRD, could be first seen when the thickness of the corrosion scale was larger due to longer exposure times. It has been suggested by Nesic, (2007) that in order to form protective corrosion scales in solutions containing Fe^{2+} below super saturated

conditions, extended exposure times are necessary. Even though the current experiment was running with Fe^{2+} concentration that was much higher than the solubility limit of $FeCO_3$ (202 mg L^{-1}), as predicted by thermodynamic calculations, long exposure times of 2324 hours were needed to see formation of a protective corrosion layer and corresponding low corrosion rates of 25 µm/year. The results from prolonged exposure times in solutions with an initial Fe^{2+} of 514 mg L^{-1} of Fe^{2+} 1300 mg L^{-1} showed a clear correlation between decreasing concentration of Fe^{2+} and decreasing corrosion rates of tested samples. It was shown that for samples tested in a solution with an initial Fe^{2+} of 514 mg L^{-1}, a decrease of Fe^{2+} concentration occurred approximately at the same time when the corrosion rate started to decrease, while for samples tested in a solution initially highly super saturated with Fe^{2+} (1300 mg L^{-1}), a decrease of Fe^{2+} was seen when a corrosion rate of 1.5 µm $year^{-1}$ was observed. It is important to emphasize that when the solution is highly super saturated with respect to $FeCO_3$, the precipitation of $FeCO_3$ will occur on all available surfaces, including the test vessel and its ancillaries, at the same time contributing to a long-term decrease in Fe^{2+} concentration and due to removed excess of HCO_3^- with the general CO_2 gas bubbling, to a long-term decrease of pH towards that predicted by thermodynamics for a solution saturated with $FeCO_3$. Consequently, observed decreasing concentration of Fe^{2+} in the solution cannot be directly used to estimate the rate of scale formation, but the time when the Fe^{2+} concentration started to decrease, as shown by current results, can be used as an indication when the protective scale starts to be formed, which is reflected in decreasing corrosion rate. Results from close packed experiments with free water volume to steel surface ratio (V/S) of 0.2 ml cm^{-2} showed that it is not the thickness of the electrolyte above the steel surface, but the Fe^{2+} concentration in the solution that influences steel corrosion rates. Despite the high V/S ratio (40 ml cm^{-2}), materials exposed to highly super saturated conditions obtained similar corrosion rates as those tested in the close packed conditions with a V/S of 0.2 ml cm^{-2} (as in the annulus of a flexible pipe). However, the V/S ratio has a significant influence on the time, which is needed to reach supersaturation of Fe^{2+} in the test solution when starting with a non Fe^{2+} containing electrolyte. With lower V/S ratio, supersaturation with Fe^{2+}, together with HCO_3^-, and the corresponding maximum pH are reached faster compared to tests executed with high V/S ratio. It has been reported by Rubin et al.3 that the maximum pH for V/S = 0.17 ml cm^{-2} was reached after 48 hours, whereas at V/S = 40 ml cm^{-2} peak values were first noticed after approximately 528 hours. Traditional electrochemical laboratory experiments are designed with a large V/S ratio (small working electrode and large volume of electrolyte) and with relatively short test times. This means that the chemistry (Fe^{2+} concentration) of the electrolyte changes slowly during the testing period and consequently the behaviour found in this work might never be experienced. It should also be emphasized that in operating conditions, findings presented in this paper, will only apply for conditions with no or low replenishment of corrosive media such as in confined conditions, which are relevant for the present case. Corrosion rates presented in this paper for highly super saturated conditions with Fe^{2+} correlated very well with former results from close packed cell tests reported in the literature3, which show that when performing closely packed cell tests, a high pH of 6.2 was obtained within 48 hours of exposure. This is negligible compared to the lifetime of a flexible pipe which is typically 20-30 years. It can therefore be assumed that from the very beginning of the operation of the pipe, steel wires, are exposed to highly supersaturated environment with Fe^{2+} during service. Consequently, it is expected that the low corrosion rate found in this investigation for highly supersaturated solutions is applicable to the annulus region for the entire life time of the flexible pipe. It has been reported (Akid, 2010) that when exposing materials to corrosive media, their fatigue life is decreased compared to the air conditions.

Consequently, the corrosive environment and the resulting corrosion behaviour of steel armours have a significant impact on the fatigue life of steel armours situated in the annulus region and consequently the fatigue performance of the entire flexible pipe. The results presented in this paper indicate that steel armours exposed to simulated annulus conditions (high initial supersaturation) only experience high corrosion rates initially, while after a short time the corrosion rate decreases to 1.5 μm/year, which has been also supported by other authors (Akid, 2010). It indicates that the corrosion process of steel armours stops relatively quickly after the water and corrosive gases (CO_2) reach the annulus region. Consequently, when the protective layer is formed and the corrosion rate decreases to almost zero, the corrosion process is expected to have lower impact on the fatigue life of steel armours, which is beneficial for the lifetime of a flexible pipe. In order to predict fatigue damage of a flexible pipe, corrosion fatigue tests of steel armours are performed on a laboratory scale. A correct simulation of the annulus conditions when performing corrosion fatigue experiments, plays an important factor not only in predicting fatigue life of a flexible pipe but also in optimizing its design. In the corrosion fatigue tests, the annulus conditions are typically simulated by exposing steel armours to solution with high initial concentration of Fe^{2+}. However, the results presented in this paper show that even small changes in the initial Fe^{2+} concentration have a significant impact on the kinetics of scale formation and accordingly how fast a decrease of corrosion rate of steel armours can be observed. Consequently, in order to ensure a close simulation of the annulus conditions when performing corrosion fatigue testing, it is important to expose steel armours to solution with high initial supersaturation of Fe^{2+}.

5 Conclusion

5.1 Analysis of Fe^{2+} evolution showed that a decrease in Fe^{2+} and corresponding pH, was directly related to a decrease in a corrosion rate of analysed samples. A twice as fast decrease in Fe^{2+} concentration and pH was observed in solutions initially highly super saturated with Fe^{2+} compared to solutions with Fe^{2+} concentration marginally above the solubility limit of $FeCO_3$.

5.2 Analysis of the Fe^{2+} together with obtained corrosion rates for samples exposed to different initial Fe^{2+}, revealed that before protective $FeCO_3$ can be formed, high supersaturation of Fe^{2+} (~1300 mg L^{-1}) needs to be built up in the solution.

5.3 Electrochemical measurements confirmed that the initial amount of Fe^{2+} in the solution had a significant impact on the corrosion rate of steel materials. Results showed that high initial supersaturation of Fe^{2+} are required for fast formation of protective layers and decrease of corrosion rates close to 1.5 μm/year.

5.4 Metallographic and diffraction analysis showed that the morphology of the scale depended on the initial exposure environment and exposure time. Samples exposed to the solution without Fe^{2+} or in super saturated solution for a short exposure time, formed scales consisting of Fe_3C embedded in $FeCO_3$, while under highly supersaturated conditions, the scale showed a double layer with an inner layer of Fe_3C embedded in $FeCO_3$ and an outer $FeCO_3$ layer.

5.5 The results from experiments performed with simulated annulus conditions (high supersaturation of Fe^{2+}) showed fast decrease of corrosion rate to 1.5 μm/year, indicating that the corrosion process stops relatively quickly after the water and CO_2 gases reaches the annulus region. The low corrosion rate of steel armours is believed to have a beneficial impact on the fatigue life of a flexible pipe.

5.6 The results showed that small changes in initial Fe^{2+} have a large impact on the corrosion rates of steel armours. Consequently, in order to correctly simulate annulus conditions, when performing

corrosion fatigue testing, high supersaturation of Fe^{2+} must be provided from the beginning of the test.

Bibliography

1. Akid, R., (2010). 'Corrosion fatigue', Shreir's Corrosion, 928-953.
2. Al-Hassan, S., Mishra, B., Olson, D. L., Salama, M. M., (1998). 'Effect of Microstructure on Corrosion of Steels in Aqueous Solutions Containing Carbon Dioxide', Corrosion, 54, 480-491.
3. Berntsen, T., Seiersten, M., Hemmingsen, T., (2013). 'Effect of $FeCO_3$ Supersaturation and Carbide Exposure on the CO_2 Corrosion Rate of Carbon Steel', Corrosion, 69, 601-613.
4. Crolet, J. L., Thevenot, N., Nesic, S., (1998). 'Role of Conductive Corrosion Products in the Protectiveness of Corrosion Layers', Corrosion, 1998, 54, 194-203.
5. Dugstad, A., (2006). 'Fundamental Aspects of CO_2 Metal Loss Corrosion - Part 1: Mechanism', NACE International, Houston, TX.
6. Dugstad, A., Borvik, L., Palencsar, S., Eikrem, P. A., (2015). 'Corrosion Testing of Steel Armour Wires in Flexible Pipes- A parametric Study', NACE International, Houston, TX, Paper 5829.
7. Gao, M., Pang, X., Gao, K., (2011). 'The growth mechanism of CO2 corrosion product films', Corros. Sci., 53, 557-568.
8. Han, J., Brown, B. N., Nesic, S., (2007). 'Investigation of the Galvanic Mechanism for Localized Carbon Dioxide Corrosion Propagation Using the Artificial Pit Technique', NACE International, Houston, TX, 2007, Paper 07323.
9. Han, J., Yang, Y., Nesic, S., Brown, B. N., (2008). 'Roles of Passivation and Galvanic Effects in Localized CO_2 Corrosion of Mild Steel', NACE International, Houston, TX, 2008, Paper 08332.
10. Kumar, A., (2008). E-Journal of Chemistry, 5; 275.
11. Maksoud, S.A.A., (2008). Int. J. Electrochem. Sci, 3; 528.
12. Mora, J. L., Turgoose, S., (2002). 'Fe$_3$C influence on the corrosion rate of mild steel in aqueous CO2 systems under turbulent flow conditions', Corros. Sci., 44, 1223–1246.
13. Nesic, S., (2007). 'Key issues related to modelling of internal corrosion of oil and gas pipelines – A review', Corros. Sci., 2007, 49, 4308-4338.
14. Nordsveen, M., Nesic, S., Nyborg, R., Stangeland, A., (2003). 'A Mechanistic Model for Carbon Dioxide Corrosion of Mild Steel in the Presence of Protective Iron Carbonate Films-Part 1: Theory and Verification', Corrosion, 59, 443-456.
15. Orubite, K., Jack, I.R., Ochei, M. O., Akaranta, J., (2007). Appl. Sci. Environ. Manage. 11: 27.
16. Rubin, A., Gudme, J., (2006). 'Qualification of Steel Wire for Flexible Pipes', NACE International, Houston, TX, Paper 06149.
17. Ueda, M., Ikeda, A., (1996).' Effect of Microstructure and Cr Content in Steel on CO_2 Corrosion', NACE International, Houston, TX, Paper 13.
18. Videm, K., Dugstad, A., (1989). 'Corrosion of carbon steel in an aqueous carbon dioxide environment. I: Solution effects', Mater. Performance, 28, 63-67.
19. Zarrouk, A., Warad, I., Hammouti, B., Dafali, A., Al-Deyab, S.S., Benchat, N., (2010). Int. J. Electrochem. Sci, 5; 1516.
20. Zhang, Y., Pang, X., Qu, S., Li, X., Gao, K., (2012). 'Discussion of the CO2 corrosion mechanism between low partial pressure and supercritical condition', Corros. Sci., 59, 186-197.